

CI-dataset and DetDSCI methodology for detecting too small and too large critical infrastructures in satellite images: Airports and electrical substations as case study

Francisco Pérez-Hernández^{a,*}, Jose Rodríguez-Ortega^a, Yassir Benhammou^a,
Francisco Herrera^a, Siham Tabik^a

^a*Andalusian Research Institute in Data Science and Computational Intelligence, University of Granada, 18071 Granada, Spain*

Abstract

The detection of critical infrastructures in large territories represented by aerial and satellite images is of high importance in several fields such as in security, anomaly detection, land use planning and land use change detection. However, the detection of such infrastructures is complex as they have highly variable shapes and sizes, i.e., some infrastructures, such as electrical substations, are too small while others, such as airports, are too large. Besides, airports can have a surface area either small or too large with completely different shapes, which makes its correct detection challenging. As far as we know, these limitations have not been tackled yet in previous works. This paper presents (1) a smart Critical Infrastructure dataset, named CI-dataset, organised into two scales, small and large scales critical infrastructures and (2) a two-level resolution-independent critical infrastructure detection (DetDSCI) methodology that first determines the spatial resolution of the input image using a classification model, then analyses the image using the appropriate detector for that spatial resolution. The present study targets two representative classes, airports and electrical substations. Our experiments show that DetDSCI methodology achieves up to 37,53% F1 improvement with respect to Faster R-CNN, one of the most influential detection models.

Keywords: Detection, Convolutional Neuronal Networks, Remote sensing images, Ortho-images

*Corresponding author

Email addresses: fperezhernandez@ugr.es (Francisco Pérez-Hernández),
jrodriguez98@correo.ugr.es (Jose Rodríguez-Ortega), benhammouyassir2@gmail.com
(Yassir Benhammou), herrera@decsai.ugr.es (Francisco Herrera), siham@ugr.es (Siham Tabik)

1. Introduction

Critical infrastructures are a type of human land use that are essential for the functioning of a society and economy [22, 26, 28]. Any threat to these facilities can cause severe problems. Examples of critical infrastructures include airports, electrical substations and harbours among others. The detection of this type of infrastructures in high resolution ortho-images is of paramount importance in several fields such as security, land use planning and change detection [5, 12, 20, 29].

Currently, deep CNNs have been largely used in the classification of high resolution ortho-images [6, 10, 28] as they achieve good accuracies specially in distinguishing infrastructures of similar scales in images of the same size and same spatial resolution. Nevertheless, the detection of critical infrastructures with dissimilar sizes and scales, e.g., electrical substations, which usually cover a surface area of the order of hundreds m^2 , versus airports, which can cover from few to hundreds km^2 , is still challenging.

Such task is addressed using remote sensing data and deep Convolutional Neural Networks (CNNs). Remote sensing data are high resolution ortho-images that can be obtained from Unmanned Aerial Vehicle (UAV) (captured at height $< 30km$ and covers from 0,1 to $100Km^2$), planes (at height $< 30km$ and covers from 10 to $100Km^2$) or satellites ($> 150km$ 10 to $1000 Km^2$) [25]. Obtaining large amounts of this type of data is expensive. Fortunately, several sources, such as Google Earth¹ and Bing Maps², allow downloading aerial and satellite images freely for the academic community. In spite of this, most existing land use datasets are prepared for training classification models and do not include annotations for training detection models.

This paper presents two-level deep learning Detection for Different Scale Critical Infrastructures (DetDSCI) methodology in ortho-images. We reformulate the problem of detecting critical infrastructures in ortho-images into two sub-problems, the detection of too small and too large scale critical infrastructures. DetDSCI methodology detects the type of infrastructure independently of its scale and consists of two stages:

- The first stage is based on a spatial resolution classification model that analyses the 2000×2000 pixels input image to estimate its zoom level and hence determine the detector to be used in the next stage.
- The second stage includes two expert detectors, one for small and the other for large critical infrastructures. Once the zoom level of the input image is determined by the first stage, the selected detector will analyse that input image according to its spatial resolution.

Addressing the detection of too small and too large scale critical infrastructures in remote sensing images independently on the spatial resolution can offer

¹Google Earth: <https://earth.google.com/web>

²Bing Maps: <https://www.bing.com/maps>

better performance. Our study targets two representative critical infrastructures, namely airports and electrical substations. As there are no public detection datasets that include both categories of critical infrastructures, we carefully built a specialised dataset, Critical Infrastructures dataset (CI-dataset). CI-dataset is organised into two subsets, Small Scale Critical Infrastructure (CI-SS) dataset with electrical substation class and Large Scale Critical Infrastructure (CI-LS) dataset with airport class.

The main contributions of this paper can be summarised as follows:

- Differently to the traditional process adopted for building most datasets, we followed a dynamic process for constructing the high quality CI-dataset organised into two scales, CI-SS for small scale critical infrastructures and CI-LS for large scale critical infrastructures. This process can be used to include more types of infrastructures. CI-dataset is available through this link³.
- We present DetDSCI methodology, a two-stages deep learning detection for dissimilar scale critical infrastructures in ortho-images. DetDSCI methodology first determines the spatial resolution of the input image then analyses it according to its spatial resolution using the appropriate expert detector. This methodology overcomes the baseline detectors trained on our high quality dataset.

This paper is organised as follows. First, a comprehensive review of related works is provided in Section 2. Our DetDSCI methodology is presented in Section 3. The dynamic process of building our CI-dataset is provided in Section 4. The experimental analysis carried out for the construction of CI-dataset and the evaluation of DetDSCI methodology are given in Section 5. Finally, conclusions and future works are given in Section 6.

2. Related works

Related works that apply deep learning on remote sensing data can be broadly divided into two types, top-down and bottom-up works:

- Top-down works, first build a large dataset with an important number of object-classes, mainly objects that can be recognised from remote sensing images, e.g., vehicles or soccer stadiums. Then, analyse these images using a deep learning classification or detection models [6, 7, 8, 10, 16, 17, 24, 28].
- Bottom-up works focus on solving one specific problem that involves one or few object classes, e.g., airports [3, 4, 18, 27, 30], trees [2, 11, 13, 23] and whales [14].

³CI-dataset: <https://dasci.es/transferecia/open-data/ci-dataset/>

Our work belongs to the second category as our final objective is to build a good detector of two specific critical infrastructures, namely, airports and electrical substations. This section provides a brief summary of the current general datasets that include some critical infrastructures, the so-called top-down works (Section 2.1) then reviews the deep learning approaches used in bottom-up works (Section 2.2).

2.1. Top-down works

Most databases provided by top-down works are multi-class datasets that include some critical infrastructures, annotated for the task of image classification, which limits their usefulness. See summary in Table 1 where only a few datasets are prepared for the task of detection.

Table 1: Characteristics of general datasets that include some critical infrastructures.

Dataset	#Classes (#Infrastructure)	#Images (#Instances)	#Image width	Source	Resolution	Annotation
LULC[28]	21 (7)	2100 (2100)	256	National Map	30cm	Classification
NWPU RESISC45[6]	45 (13)	31500 (31500)	256	Google Earth	20cm-30cm	Classification
fMoW[10]	62 (25)	523846 (132716)	N/A	OpenStreetMap	31cm-1.6m	Classification
NWPU VHR-10[7]	10 (4)	800 (3651)	~1000	Google Earth	15cm-12m	Horizontal BB
xView[16]	60 (9)	1400 (1000000)	3000	DigitalGlobe	31cm	Horizontal BB
DIOR[17]	20 (11)	23463 (192472)	800	Google Earth	30cm-50cm	Horizontal BB
DOTA[24]	15 (6)	2806 (188282)	800~4000	Google Earth	15cm-12m	Oriented BB

For example, in [28], the authors created LULC dataset organised into 21 classes. Each class contains 100 images of size 256×256 pixels. The authors in [6] provide a dataset named NWPU-RESISC45. This dataset is composed of 31.500 images of 256×256 pixels, in 45 classes with 700 images in each class. NWPU-RESISC45 includes images with a large variation in translation, spatial resolution, viewpoint, object pose, illumination, background, and occlusion. Besides, it has high within-class diversity and between-class similarity. Functional Map of the World (fMoW) [10] is a dataset containing a total of 523.846 images with a spatial resolution of 0, 31 and 1, 60 meters per pixel. It includes 62 classes with 132.716 instances from OpenStreetMap. These datasets are prepared for the image classification task and hence they are not useful for the detection task.

Examples of datasets prepared for the task of object detection are NWPU VHR-10, xView, DIOR and DOTA. NWPU VHR-10 dataset [7] is organised into 10 classes, each class contains 800 images of width 1000 pixels. It contains mainly small scale objects such as airplane, ship, storage tank, baseball diamond, tennis court, basketball court, ground track field, harbour, bridge, and vehicle. Authors on [16] presented xView dataset for detecting 60 object-classes with over 1 million instances. These classes are focused on vehicles and small scale objects and the images have a width of 3000 pixels. DIOR, a new dataset was published on [17], where 23463 images and 192472 instances covered 20 object classes. DIOR dataset has a large range of object size variations and is

focused on detection with a width on the images of 800 pixels. DOTA dataset [24] is composed of 15 classes of small scale objects with 2.806 images from Google Earth where the total instances are 188.282. The size of the images is between 800 and 4.000 pixels, and they are labelled with oriented bounding boxes. Although the last four datasets are prepared for the task of object detection, they do not focus on any specific problem as they are all types of visible objects from space. In addition, none of these datasets includes electrical substations and only DIOR includes the airport category.

2.2. Bottom-up works

A large number of bottom-up works focus on improving the detection of airports. In [30], the authors propose a method using CNNs for airport detection on optical satellite images. The proposed method consists mainly of three steps, namely, region proposal, CNN identification, and localisation optimisation. The model was tested on an image data set, including 170 different airports and 30 non-airports. All the tested optical satellite images were collected from Google Earth with a resolution of $8m \times 8m$ and a size of about 3000×3000 pixels. The method proposed in [3] first detects various regions on RSIs, then uses these candidate regions to train a CNN architecture. The sizes of the airport images were 3000×2000 pixels with a resolution of 1m. A total of 92 images were collected. In [4], the authors developed a hard example mining and weight-balanced strategy to construct a novel end-to-end convolutional neural network for airport detection. They designed a hard example mining layer to automatically select hard examples by their losses and implement a new weight-balanced loss function to optimise CNN. The authors in [27] proposed an end-to-end airport detection method based on convolutional neural networks. Additionally, a cross-optimisation strategy has been employed to achieve convolution layer sharing between the cascade region proposal networks and the subsequent multi-threshold detection networks, and this approach significantly decreased the detection time. Once the airport is detected, they use an airplane detector to obtain these instances. To address the insufficiency of traditional models in detecting airports under complicated backgrounds from remote sensing images, authors in [18] proposed an end-to-end remote sensing airport hierarchical expression and detection model based on deep transferable convolutional neural networks.

3. DetDSCI methodology: Two-level deep learning Detection for Different Scale Critical Infrastructure methodology in ortho-images

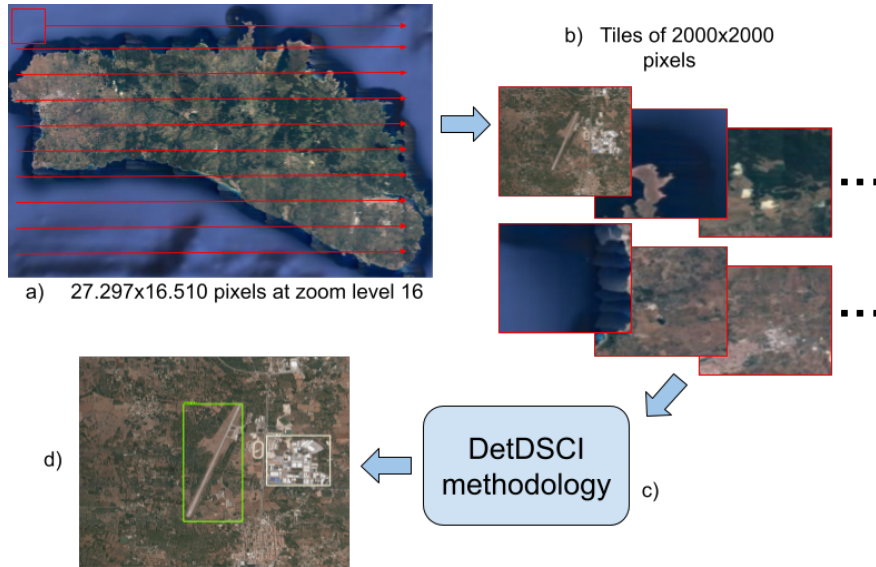


Figure 1: DetDSCI Methodology detection applied to the island of Menorca (Spain). (a) A sliding window processing approach. (b) Obtained 2000×2000 pixels crops. (c) DetDSCI methodology applied to each crop. (d) Output image with detection results.

This section presents DetDSCI methodology which aims at addressing the detection of airports and electrical substations of very dissimilar sizes and shapes in large areas represented by satellite images, see illustration in Figure 1. We define two broad ranges of spatial resolutions also called zoom levels, see correspondence between zoom level and spatial resolution in Table 2. The first range includes zoom levels in [14,17] and the second range includes zoom levels in [18,23]. These intervals have been selected experimentally as described in the next section.

Table 2: The correspondence between spatial resolution and zoom level.

Large critical infrastructures		Small critical infrastructures	
Zoom level	Spatial resolution(m^2 /pixel)	Zoom level	Spatial resolution(m^2 /pixel)
14	6.2	18	0.39
15	3.1	19	0.19
16	1.55	20	0.10
17	0.78	21	0.05
		22	0.02
		23	0.01

To reduce the number of false positives due to the differences in different zoom levels, DetDSCI methodology first distinguishes between the two zoom

level ranges then applies the corresponding detector according to the spatial resolution of each input image. In particular, DetDSCI is actually a two stages pipeline as illustrated in Figure 2. The first stage determines whether the input image belongs to the first or second zoom levels interval. Depending on the selected zoom level interval, the second stage analyses that image using the specialised detector on that specific group of critical infrastructures.

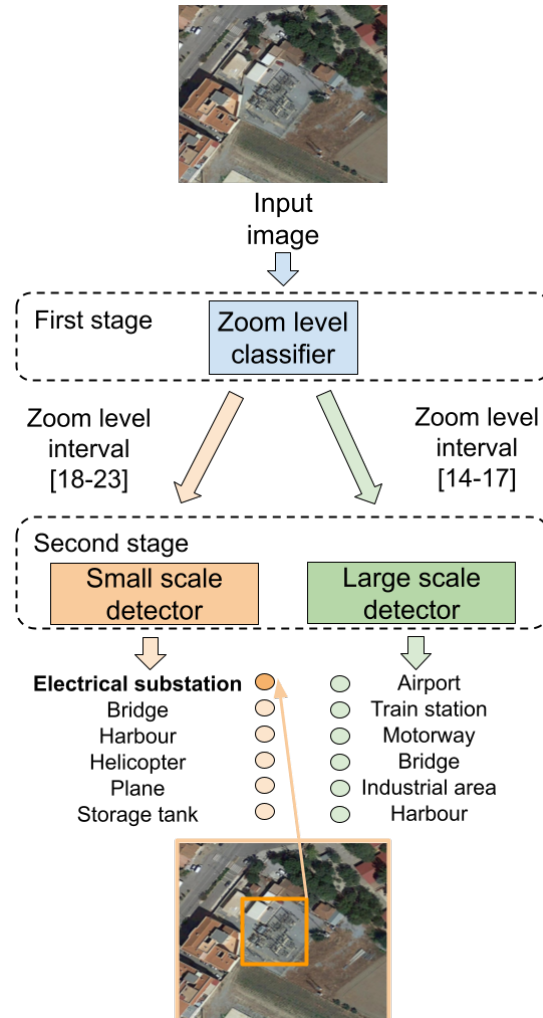


Figure 2: DetDSCI methodology.

3.1. Stage 1: Estimating the spatial resolution of the input image

To distinguish between too large and too small critical infrastructures, we consider two zoom levels intervals, [14,17] and [18,23]. Too large infrastructures can be visually recognised in 2000×2000 pixels images of zoom levels 14, 15,

16 and 17. See an example in Figure 3. While, too small scale infrastructures can be visually recognised in 2000×2000 pixels images of zoom levels 18, 19, 20, 21, 22 and 23. See an example in Figure 4.



Figure 3: Four images of El Hierro airport (latitude: 27.81402°N , longitude: $-17.88518^{\circ}\text{W}$, Canary Islands, Spain) with zoom levels 14(a), 15(b), 16(c) and 17(d), obtained from Google Maps.

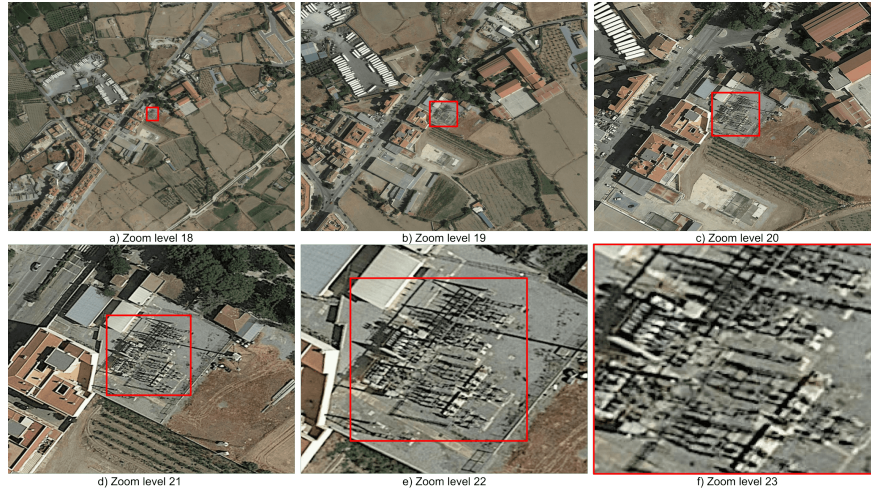


Figure 4: Six images of Guadix electrical substation (latitude: 37.30853°N , longitude: -3.12997°W , Granada, Spain) with zoom levels 18(a), 19(b), 20(c), 21(d), 22(e) and 23(f), obtained from Google Maps.

The first stage of DetDSCI distinguishes between these two intervals, large $[14,17]$ and small $[18,23]$ zoom levels interval. This stage is based on a binary classification model that analyses the input image to determine its zoom level interval and hence determines the most appropriate detector to be used in the second stage.

3.2. Stage 2: Detection of critical infrastructures

The zoom level interval estimated in the first stage will be used to guide the selection of the detector in the second stage. In particular, this stage is based on two detection models:

- The first detection model is applied to large scale infrastructures. It considers six infrastructure classes, namely airport, bridge, harbour, industrial area, motorway and train station. Figure 5 shows examples of these classes.
- The second detection model is applied to small scale infrastructures. It considers six classes, namely electrical substation, bridge, plane, harbour, storage tank and helicopter. Figure 6 shows examples of these classes.

It is worth mentioning that the inclusion of new classes in both detectors was based on the preliminary experimental study explained in the next section.



Figure 5: Examples of the classes considered by the large infrastructure detection model, left to right: airport(a), bridges(b), harbour(c), industrial area(d), motorway(e) and train station(f).

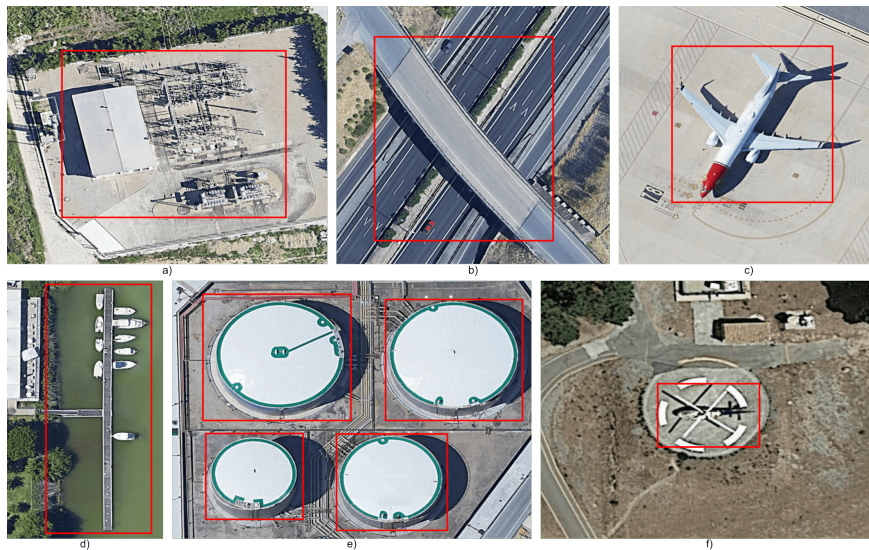


Figure 6: Examples of the classes considered in the small infrastructure detection model, left to right: electrical substation(a), bridge(b), plane(c), harbour(d), storage tanks(e) and helicopter(f).

4. CI-dataset construction guided by the performance of Faster R-CNN

It is well known that building good quality models requires good quality datasets, also called smart data [21]. The concept of smart data includes all pre-processing methods that improve value and veracity of data. In the context of object detection, usually training datasets are first built then analysed using machine learning models. This classical procedure is suitable only when the

involved objects are of similar sizes and can be correctly identified at the same spatial resolution.

To overcome these limitations, we built the critical infrastructures dataset, CI-dataset, guided by the performance of one of the most robust detectors, namely Faster R-CNN. We organised CI-dataset into two subsets, one for small scale, CI-SS and the other one for large scale, CI-LS critical infrastructures. The construction process of both subsets is dynamic and guided by the performance of Faster R-CNN detection model on the electrical substation class for CI-SS and the airport class for CI-LS. This section describes the construction process used to obtain the final high-quality CI-dataset for detecting electrical substations and airports.

The dynamic process guided by the detection model is based on three main steps:

- **Step 1: Constructing the initial set for each target class:** First, we selected the combination of zoom levels at which the airports and the electrical substations can be recognised by the human eye. Then, we downloaded images for each one of these two classes with different zoom levels. Afterwards, we selected the most suitable zoom levels combination guided by the performance of Faster R-CNN.
- **Step 2: Extending the dataset with more object classes:** We analysed all the object classes that can be confused with the target class and hence can cause false positives (FP). All these potential FP are obtained from public datasets and included in our CI-dataset. Then the performance of the model is analysed to select the final object classes to be included.
- **Step 3: Further increasing the size of the training set:** We increased the number of instances of the final classes in the training set using new images from Google Maps.

For simplicity, we named the three different versions of the training, test datasets and detection model according to the construction step as described in Table 3. At the end of this process, we obtained the final CI training and test datasets.

Table 3: The names of the training and test subsets of the CI-dataset and the corresponding detection model created at each step of the process.

	Train	Test	Detection model
Step 1	CI-SS_train_alpha	CI-SS_test_alpha	CI-SS_Det_alpha
Step 2	CI-SS_train_beta	CI-SS_test_stable	CI-SS_Det_beta
Step 3	CI-SS_train_stable	CI-SS_test_stable	CI-SS_Det_stable
Step 1	CI-LS_train_alpha	CI-LS_test_alpha	CI-LS_Det_alpha
Step 2	CI-LS_train_beta	CI-LS_test_stable	CI-LS_Det_beta
Step 3	CI-LS_train_stable	CI-LS_test_stable	CI-LS_Det_stable

4.1. Step 1: Constructing the initial set for each target class

The first process is to carefully select the zoom levels at which the considered objects fit in a 2000×2000 pixels image and can be recognised by the human eye. Ortho-images of this size can capture small scale critical infrastructures within 18 to 23 zoom levels (see Figure 6) and large scale critical infrastructures within 14 to 17 zoom levels (see Figure 5). For building CI-dataset, we used two services to visualise then download images from Google Maps, namely, SAS Planet⁴ and Google Maps API⁵.

Although all selected zoom levels provide useful information for training the detection model, the lowest, 14 and 18, and highest zoom levels, 17 and 22 and 23, require specific manual pre-processing to fit 2000×2000 pixels⁶ so that they can be used for training the detection model. For the test process, no pre-processing is applied and zoom levels 14 and 17 for large scale (Figure 7 (a)) and 18, 22 and 23 for small scale (Figure 7 (b)) infrastructures are discarded. That is, we consider zoom levels in [19,21] for the electrical substation and in [15,16] for the airport class, in the test set. Once the zoom levels are selected for the training process, the images of the target class are downloaded to build subsets CI-SS and CI-LS.

⁴SAS Planet: [//www.sasgis.org/](http://www.sasgis.org/)

⁵Google Maps API: [//https://cloud.google.com/maps-platform](https://cloud.google.com/maps-platform)

⁶Pre-processing includes fusing multiple tiles, cropping a tile and/or resizing the obtained image to 2000×2000 pixels. Notice that this size corresponds to the the input layer of the detection model.

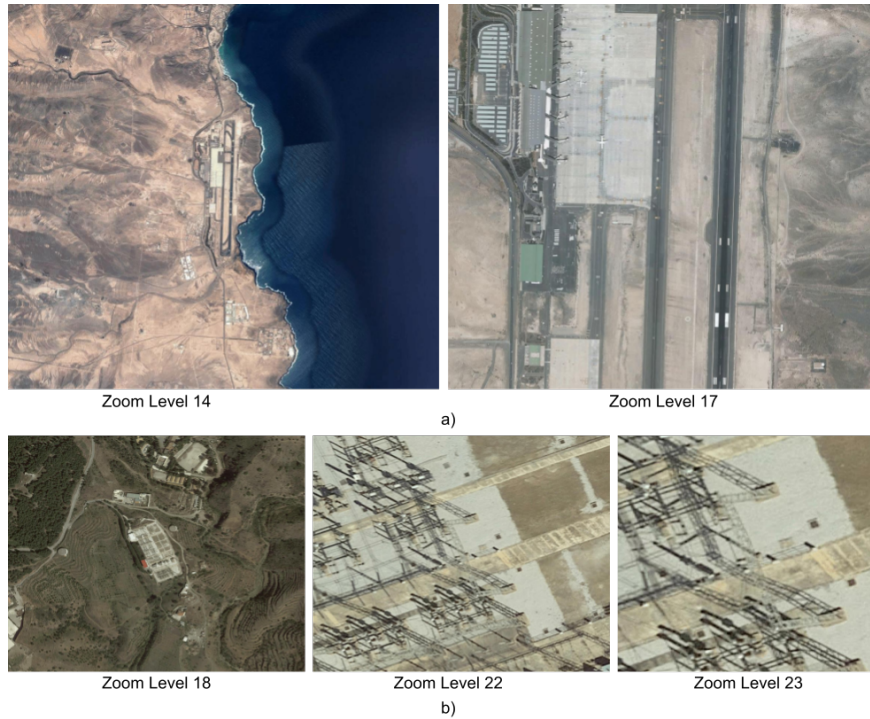


Figure 7: Zoom levels discarded for the test. a) Large scale discard 14 for having the objects too far away and 17 for occupying more of the image. b) Small scale discard 18 for having the objects too far away and 22 and 23 for occupying more of the image.

Finally, once the target class dataset is constructed, we analysed all the combinations of zoom levels to determine which one improves the learning process of the detection models. Guided by the performance of the Faster R-CNN on the target class, we discarded the zoom levels that did not help in the learning process of the detector.

Small Scale: The initial CI-SS dataset, CI-SS_train_alpha, is built using the electrical substation images with zoom levels from 18 to 23. We downloaded 550 images with different zoom levels, as shown in Table 4a. For building the test set, CI-SS_test_alpha, we downloaded 75 images of the electrical substation class with zoom levels from 19 to 21, as shown in Table 4b.

Table 4: Number of instances in the electrical substation class, a) CI-SS_train.alpha, b) CI-SS_test.alpha.

(a)	
Zoom level	Electrical substation
18	103
19	103
20	103
21	103
22	103
23	103
Total	618

(b)	
Zoom level	Electrical substation
19	27
20	27
21	27
Total	81

Large Scale: The initial version of CI-LS dataset, CI-LS_train.alpha, is built using only airport images with zoom levels from 14 to 17. We downloaded 160 images of airports from Spain and 80 airports from France, as shown in Table 5a. To build the initial test set, CI-LS_test.alpha, we downloaded 32 images of Spanish airports with two zoom levels 15 and 16, as shown in Table 5b.

Table 5: Number of instances for the airport class, a) CI-LS_train.alpha, b) CI-LS_test.alpha.

(a)	
Zoom level	Airport
14	60
15	69
16	251
17	124
Total	504

(b)	
Zoom level	Airport
15	17
16	16
Total	33

4.2. Step 2: Extending the dataset with more object classes

After a careful analysis of the FP committed by the detection model when trained on the initial dataset, we determined all potential object classes that make the detector confuse the target class with other different objects. At this stage, we analysed the impact of each one of these potential FP on the learning

of the detector and extended the dataset with more object classes from public datasets. If the performance improves, that potential FP class is maintained in the dataset, otherwise it is eliminated from the dataset.

For small scale infrastructure, the DOTA dataset will be added since their objects are of similar scales. For large scale infrastructures the DIOR dataset will be used as it contains infrastructures of similar sizes.

Small Scale: Initially, we included in CI-SS_train_beta all DOTA classes listed in Table 6. Then we eliminated each DOTA class one by one and evaluated their impact on the detector performance.

Table 6: Number of instances for small scale critical infrastructures, CI-SS_train_beta.

Zoom level	18	19	20	21	22	23	DOTA	Total
Electrical substation	103	103	103	103	103	103	-	618
Large vehicle	0	3	26	5	3	0	16923	16960
Swimming pool	111	104	62	11	2	0	1732	2022
Helicopter	0	0	0	0	0	0	630	630
Bridge	19	18	5	0	0	0	2041	2083
Plane	0	0	0	0	0	0	7944	7944
Ship	0	0	0	0	0	0	28033	28033
Soccer ball field	4	4	1	0	0	0	311	320
Basketball court	0	0	0	0	0	0	509	509
Ground track field	0	0	0	0	0	0	307	307
Small vehicle	0	0	141	234	68	5	26099	26547
Harbour	0	0	0	0	1	0	5937	5938
Baseball diamond	0	0	0	0	0	0	412	412
Tennis court	6	6	1	0	0	0	2325	2338
Roundabout	25	26	13	1	0	0	385	450
Storage tank	23	39	36	12	0	0	5024	5134

In addition, as we found that the most relevant new classes are bridge, harbour, storage tank, plane and helicopter, the detector is trained to discriminate these classes too. For building CI-SS_test_stable, we included 132 images of the five new classes, as summarised in Table 7.

Table 7: Number of instances in the final version of small scale critical infrastructures, CI-SS_test_stable dataset.

Zoom level	Electrical substation	Helicopter	Bridge	Plane	Harbour	Storage tank
19	27	8	21	68	57	136
20	27	8	15	35	27	50
21	27	6	13	17	12	24
Total	81	22	49	120	96	210

Large Scale: After analysing the FP with Faster R-CNN, we included three object classes from DIOR dataset into CI-LS_train_beta, namely train station, bridge and harbour, and built the motorway and industrial area class, see Table

8. We built a test set, CI-LS_test_stable, by including 114 new images of the five classes as it can be seen in Table 9.

Table 8: Number of instances for large scale critical infrastructures, CI-LS_train_beta dataset.

Zoom level	Airport	Train station	Motorway	Bridge	Industrial	Harbour
14	60	1	566	1	11	1
15	69	2	819	1	14	1
16	251	2	3207	8	34	1
17	124	19	2859	4	50	1
DIOR	1327	1011	-	3967	-	5509
Total	1831	1035	7451	3981	109	5513

Table 9: Number of instances the final version of large scale critical infrastructures, CI-LS_test_stable dataset.

Zoom level	Airport	Train station	Motorway	Bridge	Industrial	Harbour
15	17	25	518	115	59	32
16	16	22	303	55	27	20
Total	33	47	821	170	86	52

4.3. Step 3: Further increasing the size of the training set

In this stage, we further increase the number of all the new object classes added to both training subsets using new images from Google Maps.

Small Scale: As the CI-SS_Det_beta trained model confuses electrical substation with several elements from urban areas, we included urban areas as context in the new training images in the rest of the classes. Namely, we downloaded a total of 1173 new images. The characteristics of the resulting CI-SS_train_stable are shown in Table 10.

Table 10: Number of instances for small scale critical infrastructures, final CI-SS_train_stable dataset.

Zoom level	18	19	20	21	22	23	DOTA	19	20	21	Total
Electrical substation	103	103	103	103	103	103	-	175	164	144	1101
Swimming pool	111	104	62	11	2	0	1732	807	308	130	3267
Helicopter	0	0	0	0	0	0	630	20	17	17	684
Bridge	19	18	5	0	0	0	2041	70	34	19	2206
Plane	0	0	0	0	0	0	7944	13	8	2	7967
Soccer ball field	4	4	1	0	0	0	311	142	64	40	566
Basketball court	0	0	0	0	0	0	509	91	49	35	684
Ground track field	0	0	0	0	0	0	307	4	0	0	311
Harbour	0	0	0	0	1	0	5937	1	0	0	5939
Baseball diamond	0	0	0	0	0	0	412	2	0	0	414
Tennis court	6	6	1	0	0	0	2325	120	45	27	2530
Roundabout	25	26	13	1	0	0	385	77	25	7	559
Storage tank	23	39	36	12	0	0	5024	499	213	61	5907

Large Scale: We further increased the size of CI-LS_train_beta dataset by

including 768 new images. The characteristics of the resulting CI-LS_train_stable are shown in Table 11.

Table 11: Number of instances for large scale critical infrastructures, final CI-LS_train_stable dataset.

Zoom level	Airport	Train station	Motorway	Bridge	Industrial	Harbour
14	60	5	1012	37	69	17
15	69	6	1280	37	71	17
16	251	6	3947	57	116	27
17	124	27	4805	168	291	23
DIOR	1327	1011	-	3967	-	5509
Total	1831	1055	11044	4266	547	5593

5. Experimental study

This section provides all the performed experimental analysis to obtain CI-dataset and the evaluation of DetDSCI methodology. Section 5.1 summaries the experimental setup for the analysis. Section 5.2 provides all the detection model results obtained during the CI-dataset construction process. Finally, Section 5.3 provides the analysis and comparison of the proposed DetDSCI methodology.

5.1. Experimental setup

The dynamic construction of the dataset requires the use of a good detection model. After a careful experimental analysis, we found that Faster R-CNN is the most suitable for this study as it achieves a good speed accuracy trade-off [15].

For training the detection models, the images were resized to 2000×2000 pixels image, which represents the required size of the input layer of modern detectors. A careful selection of the zoom level is necessary so that the entire object can fit in the image.

In the experiments carried out in the next sections, we used Keras [9] as a deep learning framework for classification and TensorFlow [1] as a deep learning framework for detection.

For evaluating and comparing the performance we will use these metrics: *Precision*, *Recall* and *F1* (equation 1).

$$\begin{aligned}
 Precision &= \frac{TP}{TP + FP} \\
 Recall &= \frac{TP}{TP + FN} \\
 F1 &= 2 \times \frac{Precision \times Recall}{Precision + Recall}
 \end{aligned} \tag{1}$$

where the number of true positives (TP), false positives (FP), and false negatives (FN) is computed for each class.

The detection performance is evaluated in terms of mAP (equation 2) and mAR (equation 3) standard metrics for object detection tasks [19] given 100 output regions.

$$mAP = \frac{\sum_{i=1}^K AP_i}{K} \quad AP_i = \frac{1}{10} \sum_{r \in [0.5, \dots, 0.95]} \int_0^1 p(r) dr \quad (2)$$

$$mAR = \frac{\sum_{i=1}^K AR_i}{K} \quad AR_i = 2 \int_{0.5}^1 recall(o) do \quad (3)$$

where given K categories of elements, p represents the precision and r *recall* defines the area under the interpolated precision-recall curve for each class i . Whereas o is IoU (intersection over union) in $recall(o)$ is the corresponding recall under the recall-IoU curve for each class i .

The performance of the detection models can be improved with the use of several optimisation techniques, namely data augmentation (DA) and analysing different feature extractors (FE). The eight DA techniques used to this task are listed in Table 12 and their impact will be study on the performance of each detector.

Table 12: Data augmentation techniques by model.

Model name	Data augmentation technique
DA1	Normalize image
DA2	Random image scale
DA3	Random rgb to gray
DA4	Random adjust brightness
DA5	Random adjust contrast
DA6	Random adjust hue
DA7	Random adjust saturation
DA8	Random distort colour

Besides, we consider six feature extractors (FE) listed in Table 13 and train the models with or without the best DA techniques. We will analyse the impact of all these factors on the performance of each detection model.

Table 13: Configuration of feature extractors for different models.

Model name	Region Proposal	ResNet model	with DA
FE1	Faster R-CNN	ResNet 101 V1	No
FE2	Faster R-CNN	ResNet 101 V1	Yes
FE3	Faster R-CNN	ResNet 152 V1	No
FE4	Faster R-CNN	ResNet 152 V1	Yes
FE5	Faster R-CNN	Inception ResNet V2	No
FE6	Faster R-CNN	Inception ResNet V2	Yes

5.2. Experimental study for the construction of the CI-dataset

Section 4 provided a detailed description of the construction process of CI-dataset. This subsection provides the experimental results of the detection model at each stage of that process. The performance obtained in steps 1, 2, and 3 are respectively analysed in Section 5.2.1, 5.2.2 and 5.2.3. Finally, the experimental analysis of the use of DA techniques and different FE is provided in Section 5.2.4.

5.2.1. Analysis of step 1: Construction of the target class dataset

Once the initial CI-dataset of the target class is constructed, we analysed all the combinations of zoom levels to determine which one improves the learning process of the detection models. Guided by the performance of the detection model on the target class, we discarded the zoom levels that did not help in the learning process of the detector.

Small Scale: The performance of the first detector, CI-SS_Det_alpha, trained on different zoom level combinations shows similar results as it can be seen from Table 14. We selected the combination that provides the highest number of images, which is the one that includes all the zoom levels, 18, 19, 20, 21, 22 and 23.

Table 14: Performance of CI-SS_Det_alpha when trained on different zoom level combinations of CI-SS_train_alpha and tested on CI-SS_test_alpha dataset.

Zoom level combination	Precision	Recall	F1	mAP 0.5 electrical substation	mAP 0.5-0.95 mean	mAR 0.5-0.95 mean
18,19,20,21,22,23	96,49%	67,90%	79,71%	87,45%	48,30%	60,70%
19,20,21,22,23	93,44%	70,37%	80,28%	86,23%	51,70%	60,40%
18,19,20,21,22	91,94%	70,37%	79,72%	89,90%	48,70%	59,00%
20,21,22,23	92,31%	59,26%	72,18%	79,35%	43,50%	55,80%
19,20,21,22	89,39%	72,84%	80,27%	89,18%	51,60%	62,60%
21,22,23	82,76%	29,63%	43,64%	57,90%	28,10%	38,40%
20,21,22	89,29%	61,73%	72,99%	80,55%	44,50%	54,40%
21,22	82,35%	17,28%	28,57%	51,11%	24,50%	34,70%

Large Scale: The performance of the detection model, CI-LS_Det_alpha, in different zoom level combinations shows that the best and most stable results are obtained by the combination of these zoom levels, 14, 15, 16 and 17, as it can be seen in Table 15.

Table 15: Performance of CI-LS_Det_alpha when trained on different zoom level combinations of CI-LS_train_alpha and tested on CI-LS_test_alpha dataset.

Zoom level combination	Precision	Recall	F1	mAP 0.5 airport	mAP 0.5-0.95 mean	mAR 0.5-0.95 mean
14,15,16,17	87,76%	86,00%	86,87%	89,52%	61,30%	69,10%
14,15,16	78,85%	82,00%	80,39%	84,67%	55,50%	62,10%
15,16,17	68,42%	78,00%	72,90%	87,89%	54,50%	64,20%
15,16	87,23%	82,00%	84,54%	82,66%	51,00%	57,90%

5.2.2. Analysis of step 2: Extending the number of classes

Once the CI-dataset is extended with new classes from public datasets, we analysed whether the new classes improve the performance of the detection models.

Small Scale: As it can be seen from Table 16, eliminating the three DOTA classes, small vehicle, large vehicle and ship, improves the F1 of CI-SS_Det_beta detection model. Therefore, the final dataset CI-SS_train_stable contains 13 classes, tennis court, baseball diamond, ground track field, basketball court, soccer-ball field, roundabout and swimming pool in addition to bridge, harbour, storage tank, helicopter, plane and electrical substation.

Table 16: Results of different classes to delete from DOTA dataset trained on CI-SS_train_beta and tested on CI-SS_test_stable dataset.

Classes deleted	Precision	Recall	F1
None	88,28 %	58,38 %	70,22 %
- Small vehicle	92,61 %	59,64 %	72,53 %
- Large vehicle	90,30 %	62,44 %	73,81 %
- Ship	90,67 %	67,53 %	77,35 %
- Tennis court	88,09 %	63,00 %	73,39 %
- Baseball diamond	89,97 %	66,33 %	76,31 %
- Ground track field	87,02 %	65,77 %	74,84 %
- Basketball court	91,19 %	63,80 %	74,99 %
- Soccer-ball field	93,47 %	66,64 %	77,74 %
- Roundabout	90,48 %	65,28 %	75,70 %
- Swimming pool	90,74 %	66,55 %	76,73 %

Large Scale: The results of the detection model, CI-LS_Det_beta, trained on CI-LS_train_beta, are shown in Table 17. As it can be observed from this table, including some DIOR classes increases the mAP of the detection model on the airport class to 85,73%.

Table 17: Performance of CI-LS_Det_beta when trained on CI-LS_train_beta and tested on CI-LS_test_stable.

		CI-LS_Det_beta	
		Mean	22,03%
		Airport	85,73%
		Train station	6,98%
mAP 0.5		Motorway	4,30%
		Bridge	31,97%
		Industrial	2,87%
		Harbour	0,31%
		Mean	12,20%
mAP 0.5-0.95		Small	2,00%
		Medium	4,70%
		Large	14,40%
mAR 0.5-0.95			22,10%

5.2.3. Analysis of step 3: Increasing the size of the dataset

Once the final classes are determined, new images are included to further improve the performance of the models.

Small Scale: A comparison between CI-SS_Det_beta and the new CI-SS_Det_stable, trained on the CI-SS_train_stable (Table 10), tested on the CI-SS_test_stable (Table 7) dataset, is shown in Table 18. The performance of CI-SS_Det_alpha trained and tested only on the electrical substation is included in the table as reference as well. These results show clearly that the performance of CI-SS_Det_stable improves when increasing the size of the training dataset.

Table 18: Performance of CI-SS_Det_beta and CI-SS_Det_stable, trained on CI-SS_train_stable, tested on CI-SS_test_stable. CI-SS_Det_alpha is trained and tested only on the electrical substation class.

		CI-SS_Det_alpha (only ele. sub.)	CI-SS_Det_beta (six classes)	CI-SS_Det_stable (six classes)
		Mean	87,45%	54,21%
		Electrical substation	87,45%	78,88%
		Plane	0,00%	82,94%
mAP 0.5		Helicopter	0,00%	33,83%
		Bridge	0,00%	18,33%
		Storage tank	0,00%	83,07%
		Harbour	0,00%	58,66%
		Mean	48,30%	32,30%
mAP 0.5-0.95		Small	0,00%	15,30%
		Medium	31,80%	23,50%
		Large	49,70%	36,80%
mAR 0.5-0.95			60,70%	47,80%

For a further analysis, we analysed the TP, FP, FN, Precision, Recall and F1 as shown in Table 19. As it can be observed, CI-SS_Det_stable reduces substantially the number of FP and achieves the best F1 value. Therefore, the CI-SS_Det_stable model will be used in the rest of the paper as it provides the highest performance on our target class, electrical substation.

Table 19: TP, FP, FN, Recall, Precision and F1 in CI-SS_test_stable. CI-SS_Det_stable is trained on CI-SS_train_stable and CI-SS_Det_beta is trained on CI-SS_train_beta. For comparison purposes, CI-SS_Det_alpha is trained only on airports.

	TP	FP	FN	Precision	Recall	F1
CI-SS_Det_alpha(only ele. sub.)	117	449	7	20,67%	94,35%	33,91%
CI-SS_Det_beta(six classes)	75	124	49	37,69%	60,48%	46,44%
CI-SS_Det_stable(six classes)	112	62	12	64,37%	90,32%	75,17%

Large Scale: A comparison between CI-LS_Det_beta and the new CI-LS_Det_stable, trained on CI-LS_train_stable (Table 11), tested on CI-LS_test_stable (Table 9) dataset, is shown in Table 20. The mAP of CI-LS_Det_alpha trained and tested only on the airport class is included in the table as reference as well. As it can be seen from these results, CI-LS_Det_stable shows very similar mAP on airports than CI-LS_Det_beta but much better mAP on the rest of potential FP.

Table 20: Performance of CI-LS_Det_stable and CI-LS_Det_beta tested on CI-LS_test_stable and CI-LS_Det_alpha trained and tested only on the airport class.

		CI-LS_Det_alpha (only airports)	CI-LS_Det_beta (six classes)	CI-LS_Det_stable (six classes)
mAP 0.5	Mean	89,52%	22,03%	36,48%
	Airport	89,52%	85,73%	85,37%
	Train station	0,00%	6,98%	26,45%
	Motorway	0,00%	4,30%	5,16%
	Bridge	0,00%	31,97%	40,53%
	Industrial	0,00%	2,87%	20,96%
	Harbour	0,00%	0,31%	40,40%
mAP 0.5-0.95	Mean	61,30%	12,20%	18,80%
	Small	0,00%	2,00%	2,40%
	Medium	0,00%	4,70%	6,50%
	Large	61,30%	14,40%	23,00%
mAR 0.5-0.95		69,10%	22,10%	33,90%

A comparison with CI-LS_Det_stable trained on CI-LS_train_stable and tested on CI-LS_test_stable is provided in Table 21. In general, CI-LS_Det_stable provides the highest F1.

Table 21: Comparison of TP, FP, FN, TN, Precision, Recall and F1 of CI-LS_Det_stable trained on CI-LS_train_stable and tested on CI-LS_test_stable with CI-LS_Det_beta and CI-LS_Det_alpha. CI-LS_Det_alpha is trained and tested only on the airport class.

	TP	FP	FN	Precision	Recall	F1
CI-LS_Det_alpha (only airports)	29	19	1184	60,42%	2,39%	4,60%
CI-LS_Det_beta (six classes)	236	35	977	87,08%	19,46%	31,81%
CI-LS_Det_stable (six classes)	334	39	879	89,54%	27,54%	42,12%

5.2.4. Analysis of the improvement of the detection models

The selection of the right DA techniques and FE can surely further improve the performance of the detection model. We consider eight DA techniques listed in Table 12 and study their impact on the performance of each detector. Besides we consider six FE listed in Table 13 and train the models with or without the best DA techniques. We analyse the impact of all these factors on the performance of each detection model.

Small scale: Table 22 shows the performance of CI-SS_Det_stable when applying individually different DA techniques on CI-SS_train_stable. As it can be observed from this table, applying DA8, random distort colour, achieves the best results in this model.

Table 22: Results of the different models with a DA technique in CI-SS_train_stable and CI-SS_test_stable.

		DA1	DA2	DA3	DA4	DA5	DA6	DA7	DA8
mAP 0.5	Mean	22,26%	67,85%	66,84%	68,07%	66,45%	64,83%	64,67%	69,07%
	Electrical substation	0,01%	84,89%	83,65%	83,36%	82,35%	83,23%	82,81%	82,30%
	Plane	41,34%	83,23%	88,72%	88,08%	82,35%	88,06%	85,69%	86,70%
	Helicopter	0,02%	19,82%	16,48%	14,39%	14,99%	12,42%	10,32%	24,52%
	Bridge	15,83%	64,90%	61,18%	65,86%	62,84%	55,08%	60,38%	64,96%
	Storage tank	64,28%	90,25%	89,44%	91,66%	91,16%	91,29%	91,47%	89,88%
	Harbour	12,11%	64,02%	61,55%	65,05%	65,03%	58,79%	57,32%	66,07%
mAP 0.5-0.95	Mean	12,80%	38,70%	39,20%	39,30%	39,20%	38,80%	38,40%	39,50%
	Small	0,00%	23,30%	14,10%	24,40%	23,80%	21,80%	31,00%	13,50%
	Medium	2,60%	26,50%	25,60%	27,50%	28,70%	28,20%	26,20%	26,60%
mAR 0.5-0.95	Large	18,90%	43,70%	44,90%	44,70%	44,30%	43,60%	43,70%	45,60%
		23,50%	54,20%	54,40%	53,50%	54,70%	54,10%	52,80%	54,20%

Table 23 shows the impact of the different FE and DA on the performance of CI-SS_Det_stable. As it can be seen, in mean, the best mAP is obtained when using FE2. This detection model will be the new CI-SS_Det_stable.

Table 23: Results of different FE with or without DA techniques in CI-SS_train_stable and CI-SS_test_stable.

		FE1	FE2	FE3	FE4	FE5	FE6
mAP 0.5	Mean	65,98%	68,97%	63,16%	65,39%	65,83%	63,96%
	Electrical substation	85,00%	85,19%	83,05%	87,55%	82,73%	87,78%
	Plane	85,30%	84,43%	85,81%	80,91%	86,29%	84,96%
	Helicopter	10,39%	23,14%	6,83%	12,48%	48,03%	6,23%
	Bridge	63,16%	62,38%	48,45%	50,31%	60,54%	39,71%
	Storage tank	92,28%	88,97%	91,01%	90,89%	90,93%	91,82%
	Harbour	59,75%	69,70%	63,82%	70,22%	69,71%	73,29%
mAP 0.5-0.95	Mean	38,60%	40,20%	36,70%	37,60%	36,50%	37,60%
	Small	25,90%	13,30%	4,70%	3,10%	2,70%	3,90%
	Medium	27,90%	29,90%	23,60%	21,50%	29,70%	28,60%
mAR 0.5-0.95	Large	43,40%	46,30%	42,20%	44,50%	40,70%	42,10%
		53,10%	54,10%	51,20%	53,10%	50,70%	51,30%

Large Scale: Table 24 shows the performance of CI-LS_Det_stable when applying different DA techniques on CI-LS_train_stable. These results show that applying DA3, random rgb to gray, achieves the best detection results.

Table 24: Results of the different models with a DA technique in CI-LS_train_stable and CI-LS_test_stable.

		DA1	DA2	DA3	DA4	DA5	DA6	DA7	DA8
mAP 0.5	Mean	3,61%	35,91%	37,11%	36,98%	36,62%	35,04%	36,34%	36,98%
	Airport	19,54%	85,71%	90,31%	85,75%	90,87%	91,50%	88,18%	85,84%
	Train station	0,07%	20,72%	27,98%	26,12%	23,53%	15,84%	19,50%	23,39%
	Motorway	0,36%	4,89%	6,19%	5,92%	6,36%	5,20%	5,81%	6,63%
	Bridge	0,35%	39,44%	37,78%	40,44%	36,33%	35,92%	36,35%	45,05%
	Industrial	0,11%	17,05%	21,02%	21,05%	15,85%	15,53%	22,06%	15,04%
	Harbour	1,22%	47,64%	39,37%	42,62%	46,76%	46,24%	46,13%	45,94%
mAP 0.5-0.95	Mean	1,60%	18,50%	19,30%	18,20%	18,30%	18,50%	17,90%	17,70%
	Small	0,10%	3,40%	3,00%	7,00%	2,20%	3,50%	2,30%	5,20%
	Medium	0,00%	6,20%	7,30%	6,60%	6,30%	6,70%	6,30%	6,00%
	Large	3,00%	20,70%	22,40%	21,10%	21,70%	20,80%	21,50%	23,00%
mAR 0.5-0.95		13,10%	34,80%	34,50%	35,40%	33,40%	34,20%	34,50%	34,70%

Table 25 shows the impact of the different FE and DA on CI-LS_Det_stable. One can see that FE5 obtains the best performance with Inception ResNet V2 without DA techniques. This model will be the new CI-LS_Det_stable in the rest of the paper.

Table 25: Results of different FE with or without DA techniques in CI-LS_train_stable and CI-LS_test_stable.

		FE1	FE2	FE3	FE4	FE5	FE6
mAP 0.5	Mean	36,48%	37,52%	37,67%	38,05%	42,34%	40,98%
	Airport	85,37%	86,46%	84,03%	87,70%	86,01%	87,21%
	Train station	26,45%	24,17%	34,20%	22,31%	27,76%	22,43%
	Motorway	5,16%	5,53%	4,80%	5,77%	5,95%	8,01%
	Bridge	40,53%	47,81%	36,69%	48,86%	57,27%	54,25%
	Industrial	20,96%	17,43%	23,53%	17,54%	23,64%	22,38%
	Harbour	40,40%	43,71%	42,78%	46,13%	53,41%	51,63%
mAP 0.5-0.95	Mean	18,80%	18,30%	18,80%	18,50%	20,30%	20,10%
	Small	2,40%	5,70%	3,20%	6,50%	9,70%	7,70%
	Medium	6,50%	7,30%	6,30%	6,70%	8,50%	7,20%
	Large	23,00%	21,60%	22,00%	22,90%	22,50%	22,40%
mAR 0.5-0.95		33,90%	36,30%	35,10%	35,20%	35,20%	37,70%

5.3. Experimental study of DetDSCI methodology

Once CI-dataset is constructed and the final models are trained on the small and the large scale critical infrastructures, we develop the zoom level classifier for the DetDSCI methodology. The construction of the zoom level classifier is presented in Section 5.3.1 and the analysis of DetDSCI methodology is shown in Section 5.3.2.

5.3.1. Construction of the zoom level classifier

In the first stage of DetDSCI methodology, a zoom level classifier analyses the input image and determines the scale of this input. This stage can be addressed either by identifying the specific zoom level of each input image or by identifying intervals of zoom levels.

In particular, we developed and analysed two classification models, the first one is trained on ten zoom level classes, from 14 to 23, and the second classification model is trained on two zoom level intervals, interval [14,17] and [18,23].

Table 26 shows the number of images used to train and test these two classification models. The used images were selected from datasets CI-SS_train_stable, CI-SS_test_stable, CI-LS_train_stable and CI-LS_test_stable.

Table 26: Number of images by zoom level used for training and evaluating the classifiers.

	14	15	16	17	18	19	20	21	22	23
Train	252	400	1256	2984	200	591	1080	2268	6406	663
Test	19	52	52	19	44	304	304	304	19	19

The confusion matrix for the classification by individual zoom level is shown in Table 27. The overall accuracy of this model is 68,31%, which is very low.

Table 27: Confusion matrix for the classifier by zoom level individually.

Zoom level	14	15	16	17	18	19	20	21	22	23
14	0	13	5	0	0	0	0	0	1	0
15	0	14	34	2	0	0	0	2	0	0
16	0	0	25	26	0	0	1	0	0	0
17	0	0	1	18	0	0	0	0	0	0
18	0	0	0	33	0	8	2	0	1	0
19	1	0	0	9	0	209	69	12	4	0
20	0	0	0	0	0	12	224	57	11	0
21	0	0	0	2	0	1	6	268	25	2
22	0	0	0	0	0	0	0	2	17	0
23	0	0	0	0	0	0	0	1	18	0

The confusion matrix for the classification by interval is shown in Table 28. This model obtains an accuracy of 96,83%, which is substantially higher than the classification by individual zoom level. Therefore, we selected this classifier to be included in our DetDSCI methodology.

Table 28: Confusion matrix for the classifier by zoom level by group.

Zoom level	[14,17]	[18,23]
[14,17]	134	8
[18,23]	28	966

5.3.2. Analysis of DetDSCI methodology

In this section, we analyse and compare the performance of DetDSCI methodology against the baseline detectors CI-LS_Det_stable and CI-SS_Det_stable and a baseline detector, Base_Det, trained on all the data and zoom levels.

The characteristic of each model is:

- **Base_Det:** is a Faster R-CNN ResNet 101 V1 trained on all the data at all zoom levels from CI-SS_train_stable and CI-LS_train_stable.

- **CI-LS_Det_stable:** is a Faster R-CNN Inception ResNet V2 trained on the CI-LS_train_stable dataset.
- **CI-SS_Det_stable:** is a Faster R-CNN ResNet 101 V1 with DA techniques trained on the CI-SS_train_stable dataset.
- **DetDSCI methodology:** is the methodology by which each input image is classified by the zoom level classifier and based on the output of this classifier, the detector to be used is selected between CI-LS_Det_stable or CI-SS_Det_stable.

We tested the four models on the images of the target classes, electrical substation from CI-SS_test_stable and airport from CI-LS_test_stable. The results in terms of TP, FP, FN, Precision, Recall and F1 are shown in Table 29.

Table 29: Performance comparison between DetDSCI methodology, Base_Det, CI-LS_Det_stable and CI-SS_Det_stable when tested on the fusion of CI-SS_test_stable and CI-LS_test_stable.

	TP	FP	FN	Precision	Recall	F1
Base_Det	70	35	44	66,67%	61,40%	63,93%
CI-LS_Det_stable	27	3	88	90,00%	23,48%	37,24%
CI-SS_Det_stable	71	32	44	68,93%	61,74%	65,14%
DetDSCI methodology	83	24	32	77,57%	72,17%	74,77%

As it can clearly see from this table, DetDSCI methodology overcomes Base_Det, CI-SS_Det_stable and CI-LS_Det_stable in all the aspects by achieving the highest performance. In particular, DetDSCI methodology achieves an improvement in F1 of up to 37,53%.

6. Conclusions and future work

The detection of critical infrastructures in satellite images is a very challenging task due to the large scale and shapes differences, some infrastructures are too small, e.g., electrical substations, while others are too large, i.e., airports. This work addressed this problem by building the high quality dataset, CI-dataset, organised into two subsets, CI-SS and CI-LS and using DetDSCI methodology. The construction process of CI-SS and CI-LS was guided by the performance of the detectors on electrical substations and airports respectively.

DetDSCI methodology is a two-stage based approach that first identifies the zoom level of the input image using a classifier and then analyses that image with the corresponding detection model, CI-LS_Det_stable or CI-SS_Det_stable. DetDSCI methodology achieves the highest performance with respect to the baseline detectors not only in the target objects but also in the rest of infrastructure classes included in the dataset.

As conclusions, the proposed datasets and methodology are the best solution for addressing the problem of different and dissimilar scale critical infrastructures detection in remote sensing images. This approach can be easily extended to more critical infrastructures.

As a future work, we will extend the dataset and methodology to more critical infrastructures and design a strategy to group sets of classes according to their zoom level and shared features, with the objective to achieve more robust detection models.

Acknowledgements

This work was partially supported by projects P18-FR-4961 (BigDDL-CET) and A-TIC-458-UGR18 (DeepL-ISCO). S. Tabik was supported by the Ramon y Cajal Programme (RYC-2015-18136).

References

- [1] Martín Abadi, Ashish Agarwal, Paul Barham, Eugene Brevdo, Zhifeng Chen, Craig Citro, Greg S Corrado, Andy Davis, Jeffrey Dean, Matthieu Devin, et al. Tensorflow: Large-scale machine learning on heterogeneous distributed systems. *arXiv preprint arXiv:1603.04467*, 2016.
- [2] Kristian Skau Bjerreskov, Thomas Nord-Larsen, and Rasmus Fensholt. Classification of nemoral forests with fusion of multi-temporal sentinel-1 and 2 data. *Remote Sensing*, 13(5):950, 2021.
- [3] Ümit Budak, Abdulkadir Şengür, and Uğur Halici. Deep convolutional neural networks for airport detection in remote sensing images. In *2018 26th Signal Processing and Communications Applications Conference (SIU)*, pages 1–4. IEEE, 2018.
- [4] Bowen Cai, Zhiguo Jiang, Haopeng Zhang, Danpei Zhao, and Yuan Yao. Airport detection using end-to-end convolutional neural network with hard example mining. *Remote Sensing*, 9(11):1198, 2017.
- [5] Manuel Carranza-García, Jorge García-Gutiérrez, and José C Riquelme. A framework for evaluating land use and land cover classification using convolutional neural networks. *Remote Sensing*, 11(3):274, 2019.
- [6] Gong Cheng, Junwei Han, and Xiaoqiang Lu. Remote sensing image scene classification: Benchmark and state of the art. *Proceedings of the IEEE*, 105(10):1865–1883, 2017.
- [7] Gong Cheng, Junwei Han, Peicheng Zhou, and Lei Guo. Multi-class geospatial object detection and geographic image classification based on collection of part detectors. *ISPRS Journal of Photogrammetry and Remote Sensing*, 98:119–132, 2014.

- [8] Gong Cheng, Peicheng Zhou, and Junwei Han. Learning rotation-invariant convolutional neural networks for object detection in vhr optical remote sensing images. *IEEE Transactions on Geoscience and Remote Sensing*, 54(12):7405–7415, 2016.
- [9] François Chollet et al. Keras, 2015.
- [10] Gordon Christie, Neil Fendley, James Wilson, and Ryan Mukherjee. Functional map of the world. In *Proceedings of the IEEE Conference on Computer Vision and Pattern Recognition*, pages 6172–6180, 2018.
- [11] Neil Flood, Fiona Watson, and Lisa Collett. Using a u-net convolutional neural network to map woody vegetation extent from high resolution satellite imagery across queensland, australia. *International Journal of Applied Earth Observation and Geoinformation*, 82:101897, 2019.
- [12] Daniel Guidici and Matthew L Clark. One-dimensional convolutional neural network land-cover classification of multi-seasonal hyperspectral imagery in the san francisco bay area, california. *Remote Sensing*, 9(6):629, 2017.
- [13] Emilio Guirado, Domingo Alcaraz-Segura, Javier Cabello, Sergio Puertas-Ruíz, Francisco Herrera, and Siham Tabik. Tree cover estimation in global drylands from space using deep learning. *Remote Sensing*, 12(3):343, 2020.
- [14] Emilio Guirado, Siham Tabik, Marga L Rivas, Domingo Alcaraz-Segura, and Francisco Herrera. Whale counting in satellite and aerial images with deep learning. *Scientific reports*, 9(1):1–12, 2019.
- [15] Jonathan Huang, Vivek Rathod, Chen Sun, Menglong Zhu, Anoop Korattikara, Alireza Fathi, Ian Fischer, Zbigniew Wojna, Yang Song, Sergio Guadarrama, et al. Speed/accuracy trade-offs for modern convolutional object detectors. In *Proceedings of the IEEE conference on computer vision and pattern recognition*, pages 7310–7311, 2017.
- [16] Darius Lam, Richard Kuzma, Kevin McGee, Samuel Dooley, Michael Laielli, Matthew Klaric, Yaroslav Bulatov, and Brendan McCord. xvnet: Objects in context in overhead imagery. *arXiv preprint arXiv:1802.07856*, 2018.
- [17] Ke Li, Gang Wan, Gong Cheng, Liqiu Meng, and Junwei Han. Object detection in optical remote sensing images: A survey and a new benchmark. *ISPRS Journal of Photogrammetry and Remote Sensing*, 159:296–307, 2020.
- [18] Shuai Li, Yuelei Xu, Mingming Zhu, Shiping Ma, and Hong Tang. Remote sensing airport detection based on end-to-end deep transferable convolutional neural networks. *IEEE Geoscience and Remote Sensing Letters*, 16(10):1640–1644, 2019.

- [19] Tsung-Yi Lin, Michael Maire, Serge Belongie, James Hays, Pietro Perona, Deva Ramanan, Piotr Dollár, and C Lawrence Zitnick. Microsoft coco: Common objects in context. In *European conference on computer vision*, pages 740–755. Springer, 2014.
- [20] Shengjie Liu, Zhixin Qi, Xia Li, and Anthony Gar-On Yeh. Integration of convolutional neural networks and object-based post-classification refinement for land use and land cover mapping with optical and sar data. *Remote Sensing*, 11(6):690, 2019.
- [21] Julián Luengo, Diego García-Gil, Sergio Ramírez-Gallego, Salvador García, and Francisco Herrera. Big data preprocessing. *Cham: Springer*, 2020.
- [22] Barak Oshri, Annie Hu, Peter Adelson, Xiao Chen, Pascaline Dupas, Jeremy Weinstein, Marshall Burke, David Lobell, and Stefano Ermon. Infrastructure quality assessment in africa using satellite imagery and deep learning. In *Proceedings of the 24th ACM SIGKDD International Conference on Knowledge Discovery & Data Mining*, pages 616–625, 2018.
- [23] Anastasiia Safonova, Emilio Guirado, Yuriy Maglinets, Domingo Alcaraz-Segura, and Siham Tabik. Olive tree biovolume from uav multi-resolution image segmentation with mask r-cnn. *Sensors*, 21(5):1617, 2021.
- [24] Gui-Song Xia, Xiang Bai, Jian Ding, Zhen Zhu, Serge Belongie, Jiebo Luo, Mihai Datcu, Marcello Pelillo, and Liangpei Zhang. Dota: A large-scale dataset for object detection in aerial images. In *Proceedings of the IEEE Conference on Computer Vision and Pattern Recognition*, pages 3974–3983, 2018.
- [25] Tian-Zhu Xiang, Gui-Song Xia, and Liangpei Zhang. Mini-uav-based remote sensing: techniques, applications and prospectives. *preprint*, 2018.
- [26] Zhifeng Xiao, Yiping Gong, Yang Long, Deren Li, Xiaoying Wang, and Hua Liu. Airport detection based on a multiscale fusion feature for optical remote sensing images. *IEEE Geoscience and Remote Sensing Letters*, 14(9):1469–1473, 2017.
- [27] Yuelei Xu, Mingming Zhu, Shuai Li, Hongxiao Feng, Shiping Ma, and Jun Che. End-to-end airport detection in remote sensing images combining cascade region proposal networks and multi-threshold detection networks. *Remote Sensing*, 10(10):1516, 2018.
- [28] Yi Yang and Shawn Newsam. Bag-of-visual-words and spatial extensions for land-use classification. In *Proceedings of the 18th SIGSPATIAL international conference on advances in geographic information systems*, pages 270–279, 2010.
- [29] Ce Zhang, Isabel Sargent, Xin Pan, Huapeng Li, Andy Gardiner, Jonathon Hare, and Peter M Atkinson. Joint deep learning for land cover and land use classification. *Remote sensing of environment*, 221:173–187, 2019.

- [30] Peng Zhang, Xin Niu, Yong Dou, and Fei Xia. Airport detection on optical satellite images using deep convolutional neural networks. *IEEE Geoscience and Remote Sensing Letters*, 14(8):1183–1187, 2017.